

# Selective Propylene Oxidation to Acrolein by Gold Dispersed on MgCuCr<sub>2</sub>O<sub>4</sub> Spinel

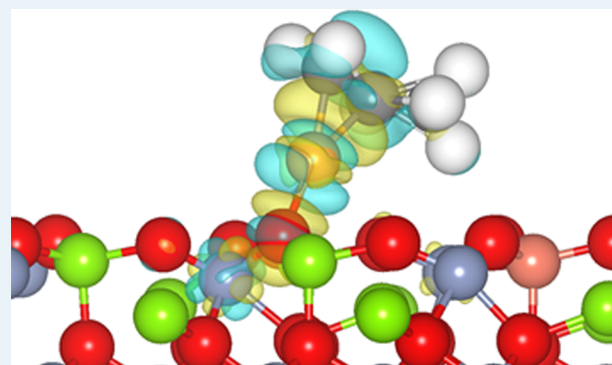
Weiyu Song,<sup>†</sup> Dulce M. Perez Fernandez,<sup>‡</sup> Lennart van Haandel,<sup>†</sup> Peng Liu,<sup>†,§</sup> T. Alexander Nijhuis,<sup>‡</sup> and Emiel J. M. Hensen\*,<sup>†</sup>

<sup>†</sup>Laboratory of Inorganic Materials Chemistry, Schuit Institute of Catalysis, <sup>‡</sup>Laboratory of Chemical Reaction Engineering, Eindhoven University of Technology, Den Dolech 2, 5612 AZ Eindhoven, The Netherlands

## S Supporting Information

**ABSTRACT:** Gold nanoparticles supported on a MgCuCr<sub>2</sub>O<sub>4</sub> spinel catalyze the aerobic oxidation of propylene to acrolein. At 200 °C, the selectivity is 83% at a propylene conversion of 1.6%. At temperatures above 220 °C, propylene combustion dominates. The good performance of Au/MgCuCr<sub>2</sub>O<sub>4</sub> in selective propylene oxidation is due to the synergy between metallic Au and surface Cu<sup>+</sup> sites. Kinetic experiments (H<sub>2</sub> addition, N<sub>2</sub>O replacing O<sub>2</sub>) show that the reaction involves molecular oxygen. DFT calculations help to identify the reaction mechanism that leads to acrolein. Propylene adsorbs on a single Au atom. The adsorption of propylene via its π-bond on gold is very strong and can lead to the dissociation of the involved Au atom from the initial Au cluster. This is, however, not essential to the reaction mechanism. The oxidation of propylene to acrolein involves the oxidation of an allylic C–H bond in adsorbed propylene by adsorbed O<sub>2</sub>. It results in OOH formation. The resulting CH<sub>2</sub>–CH–CH<sub>2</sub> intermediate coordinates to the Au atom and a support O atom. A second C–H oxidation step by a surface O atom yields adsorbed acrolein and an OH group. The hydrogen atom of the OH group recombines with OOH to form water and a lattice O atom. The desorption of acrolein is the most difficult step in the reaction mechanism. It results in a surface oxygen vacancy in which O<sub>2</sub> can adsorb. The role of Cu in the support surface is to lower the desorption energy of acrolein.

**KEYWORDS:** gold, copper, spinel support, selective oxidation, propylene, acrolein, mechanism



## 1. INTRODUCTION

The oxidation of alkenes constitutes a very important class of reactions in the chemical industry because the oxidized products are used to manufacture a wide range of commodities. Ethylene can be directly epoxidized into ethylene oxide by molecular oxygen, which is practiced at industrial scale using an optimized silver catalyst.<sup>1</sup> Propylene oxide is also an important bulk chemical obtained via more involved routes from the corresponding olefin.<sup>2</sup> Propylene also serves as the feedstock for other industrially important chemicals. Acrolein (C<sub>3</sub>H<sub>4</sub>O), the product of allylic C–H oxidation of propylene, is an intermediate in the synthesis of methionine (annual global demand of 730 000 tons in 2008) as well as in the production of acrylic acid (annual global demand of 3 400 000 tons in 2007).<sup>2</sup> Acrolein is currently produced by direct oxidation of propylene over bismuth–molybdate-based catalysts, first patented by Sohio in the 1960s.<sup>3</sup> This catalyst has been thoroughly studied, and several patents have been released using combinations of mixed-metal oxides together with bismuth and molybdenum. Nowadays, typical acrolein selectivities between 85 and 90% are obtained at 93–98% propylene conversion. The lifetime of these catalysts can reach 10 years. Industrially, the oxidation of propylene is carried out

in fixed-bed multitubular reactor at near atmospheric pressure and 330 °C. The fact that air can be used as an oxidant reduces operation costs.<sup>2</sup>

Before the Bi–Mo catalyst was discovered, copper oxide was used for the direct oxidation to acrolein by Shell.<sup>4,5</sup> From Table 1, it follows that acrolein and propylene oxide are the typical products of the oxidation of propylene over Cu-containing catalysts. The selectivity is determined by the Cu oxidation state. Cu<sup>0</sup> strongly adsorbs propylene and is therefore active for the epoxidation of propylene to propylene oxide.<sup>6,7</sup> The mechanism proposed for the epoxidation over copper catalysts involves an oxametallacyclic surface intermediate that has also been proposed as intermediate in silver-catalyzed oxidation.<sup>8,9</sup> The oxametallacycle is favorably converted to the epoxide due to the lower basicity of oxygen atoms on metallic Cu compared to Ag.<sup>9</sup> The drawback of the use of metallic Cu is its tendency to be readily oxidized to CuO or Cu<sub>2</sub>O under reaction conditions. Therefore, the Cu oxidation state is highly dependent on the propylene to oxygen ratio and the reaction

Received: October 31, 2014

Revised: January 3, 2015

Published: January 5, 2015

**Table 1.** Literature Studies about Partial Oxidation of Propylene to Acrolein over Au and Cu-Containing Catalysts<sup>a</sup>

paper	catalyst	T (°C)	GHSV (mL g <sub>cat</sub> <sup>-1</sup> h <sup>-1</sup> )	X <sub>propylene</sub> (%)	major product (S, %)	gases
Adams, 5	Cu <sub>2</sub> O	300–400	167 <sup>b</sup>	10–12	acrolein (60–85)	O <sub>2</sub>
Cant, 17	Au/SiO <sub>2</sub>	285	1500	10	acrolein (50)	O <sub>2</sub>
Sinfelt, 15	CuAu/SiO <sub>2</sub>	265–305	208–1042 <sup>c</sup>	40	acrolein (50–70)	O <sub>2</sub>
Gasior, 18	Au/SiO <sub>2</sub>	200	3750 <sup>c</sup>	2.8	acetaldehyde (75)	H <sub>2</sub> /O <sub>2</sub>
Vaughan, 7	Cu/SiO <sub>2</sub>	320	30 000	9	acrolein (35)	O <sub>2</sub>
Chu, 19	CuO <sub>x</sub> /SBA-15	227–350	18 000	1–12	PO (15–50)	O <sub>2</sub>
Llorca, 16	CuAu/TiO <sub>2</sub>	300	12 000–36 000	2.5	PO (50)	N <sub>2</sub> O
Suo, 20	Au/SiO <sub>2</sub>	325	6250 <sup>c</sup>	1	acrolein (77)	air
	Au/TiO <sub>2</sub>	325	3950 <sup>d</sup>	0.80	acrolein (20)	air
Tuysuz, 10	Cu/SBA-15	475–500	7500–15 000	20	acrolein (50)	O <sub>2</sub>
Bracey, 1	CuAu/SiO <sub>2</sub>	300	23 440 <sup>c</sup>	0.63	acrolein (81)	H <sub>2</sub> /O <sub>2</sub>
				0.23	acrolein (81)	O <sub>2</sub>
				10	acrolein (89)	H <sub>2</sub> /O <sub>2</sub>
Belin, 14	CuAu/SiO <sub>2</sub>	320	23 440 <sup>c</sup>			

<sup>a</sup>Original values of space velocity are given in h<sup>-1</sup>. <sup>b</sup>Converted from h<sup>-1</sup> to mL g<sub>cat</sub><sup>-1</sup> h<sup>-1</sup> using assumed a bed density of 2.16. <sup>c</sup>Converted from h<sup>-1</sup> to mL g<sub>cat</sub><sup>-1</sup> h<sup>-1</sup> using assumed a bed density of 0.9. <sup>d</sup>Converted from h<sup>-1</sup> to mL g<sub>cat</sub><sup>-1</sup> h<sup>-1</sup> using assumed a bed density of 1.52.

temperature.<sup>10,11</sup> Another problem, inherent to many oxidation reactions, is the high reactivity of the partial oxidation product. As a result, high selectivities can be obtained only at low conversion.<sup>12</sup> In its oxidized form, Cu is capable of abstracting one of the allylic hydrogen atoms from propylene. It has been reported that Cu<sup>2+</sup> (CuO) favors the complete combustion of propylene to CO<sub>2</sub>,<sup>11,13</sup> whereas Cu<sup>+</sup> (Cu<sub>2</sub>O) is more selective in the partial oxidation of propylene to acrolein.<sup>10,11,14</sup>

Recently, the interest in using Cu for the oxidation of propylene has been revived via the use of bimetallic CuAu catalysts. Sinfelt and Barnett already reported several decades ago that CuAu can convert propylene with reasonable selectivity to acrolein using molecular oxygen.<sup>15</sup> Llorca et al. found that CuAu supported on titania can epoxidize propylene using nitrous oxide.<sup>16</sup> The group of Hutchings investigated the synthesis of supported CuAu catalysts in more detail.<sup>1,14</sup> In their active state for propylene oxidation, CuAu catalysts contain metallic gold as well as well-dispersed copper oxide, the latter being suspected as the origin of the high selectivity to acrolein. Table 1 provides an overview of the main developments in the oxidation of propylene using Au, Cu, and bimetallic Cu–Au catalysts.

It is worthwhile to briefly mention that CuAu catalysts have recently also been used for the oxidation of ethanol to acetaldehyde. Bauer et al. reported a high ethanol conversion with very high acetaldehyde selectivity (80–90%) using CuAu nanoparticle core–shell structures for this reaction.<sup>21</sup> These authors contended that the active phase consists of a gold core with a CuO<sub>x</sub> shell in which the O binding energy is lowered, yet they also mentioned the importance of the interfacial site between gold and CuO<sub>x</sub>. Recently, some of us explored the use of Cu-containing spinel supports for gold nanoparticles. Gold nanoparticles (AuNP) dispersed on a MgCuCr<sub>2</sub>O<sub>4</sub> spinel were shown to be very active, selective, and stable in the aerobic ethanol oxidation to acetaldehyde.<sup>22</sup> For ethanol oxidation, a substantial synergy between AuNP and the Cu sites in the spinel support was observed.

The aim of the present study was to understand in more detail the formation of acrolein during propylene oxidation by gold nanoparticles deposited on a MgCuCr<sub>2</sub>O<sub>4</sub> support. The results show that there is considerable synergy between gold and the Cu ions in the surface of the mixed spinel support. The role of Cu, the oxidant (O<sub>2</sub> vs N<sub>2</sub>O), and the presence of H<sub>2</sub> in the feed on the activity and selectivity in the oxidation of

propylene was evaluated by catalytic activity measurements. DFT calculations were carried out to understand the mechanism of propylene oxidation to acrolein and the role of the support, namely, the role of Cu. The combined experimental and theoretical efforts provide new insight into the role of the metal–support interactions for a complex oxidation reaction such as that of propylene.

## 2. METHODS

**2.1. Experimental Methods.** Mg<sub>0.75</sub>Cu<sub>0.25</sub>Cr<sub>2</sub>O<sub>4</sub> (denoted as MgCuCr<sub>2</sub>O<sub>4</sub>) and MgCr<sub>2</sub>O<sub>4</sub> were prepared by a coprecipitation–calcination method using the corresponding metal nitrates as precursors. The pH of an aqueous mixed metal nitrate solution with a Mg(NO<sub>3</sub>)<sub>2</sub>/Cu(NO<sub>3</sub>)<sub>2</sub>/Cr(NO<sub>3</sub>)<sub>3</sub> ratio of 3/1/8 (for preparation of MgCr<sub>2</sub>O<sub>4</sub>, Mg(NO<sub>3</sub>)<sub>2</sub> and Cr(NO<sub>3</sub>)<sub>3</sub> were used in 1/2 ratio) was adjusted to ~11 by dropwise addition of a 1 M NaOH solution to ensure complete precipitation. The precipitate was filtered, washed, and dried at 110 °C overnight and calcined at 700 °C in air for 8 h to yield the spinel product. Gold nanoparticles were loaded on this support by homogeneous deposition–precipitation using urea as the precipitation agent. The gold loading was 1 wt %. The catalysts were calcined in air at 350 °C for 5 h.

XRD was performed on a Bruker Endeavor D4 with Cu K $\alpha$  radiation (40 kV and 30 mA). TEM imaging was performed with a FEI Tecnai 20 electron microscope at an acceleration voltage of 200 kV with a LaB6 filament. The average Au particle size was calculated by counting ~200 Au particles visible in the TEM images. The surface area was determined by N<sub>2</sub> porosimetry using a Tristar 3000 automated gas absorption system. The samples were degassed at 180 °C for 3 h prior to analyze, and the BET method was used to calculate the surface area. The gold loading of the catalysts was determined by ICP–OES. After an aliquot of the sample was treated in a mixture of HCl/HNO<sub>3</sub> (3/1), the residual solid was filtered and washed completely with demineralized water until the filtrate was 100 mL in volume.

The catalytic oxidation of propylene was performed in an atmospherically operated packed-bed quartz reactor with an inner diameter of 4 mm. In a typical test, 150 mg of catalyst was loaded into the reactor, and the flow was adjusted to 25 mL min<sup>-1</sup> (GHSV = 10 000 mL g<sub>cat</sub><sup>-1</sup> h<sup>-1</sup>). Prior to reaction, the catalyst was calcined in situ at 300 °C under 10 vol % O<sub>2</sub> for 1 h, followed by 1 h of reduction, also at 300 °C, with 10 vol %

$H_2$ . Cycles of 5 h of reaction with an intermediate regeneration by oxidation and reduction were performed. The standard feed composition used was 10/10/80 by volume of  $O_2/C_3H_6/He$ . In addition, the influence of the presence of hydrogen in the gas stream was analyzed by using a mixture of  $H_2/O_2/C_3H_6/He$  with a volume ratio of 10/10/10/70. The temperature of the reaction was controlled by a tubular oven and varied between 150 and 300 °C, according to the experiment. To evaluate the stability of the catalyst, the reaction at 200 °C was repeated after several reaction cycles. The oxidation of propylene with  $N_2O$  was also studied with a flow rate of 20 mL min<sup>-1</sup> (GHSV = 8000 mL g<sub>cat</sub><sup>-1</sup> h<sup>-1</sup>) and a concentration of propylene and  $N_2O$  of 9.3 vol % each. The outlet gases of the reaction were analyzed every 5 min by an online Compact GC (Interscience) equipped with a Rt-Q-Bond column and a Molsieve 5A column in two separate channels, both with a thermal conductivity detector (TCD). The propylene conversion ( $X$ ) and selectivity ( $S_{ac}$ ) to acrolein and the other byproducts were calculated considering the reaction  $nC_3H_6 \rightarrow mC_x$  and according to the following equations:

$$X(\%) = \frac{\sum \frac{n}{m} P_x}{P_{C_3H_6}^{\text{out}} + \sum \frac{n}{m} P_x} \times 100 = \frac{\sum \frac{n}{m} P_x}{P_{C_3H_6}^{\text{in}}} \times 100 \quad (1)$$

$$S_x(\%) = \frac{\frac{n}{m} P_x}{\sum \frac{n}{m} P_x} \times 100 \quad (\text{eq 2})$$

where  $P_x$  is the partial pressure of the carbon-containing products obtained during the oxidation of propylene (acrolein, acetone, propylene oxide, propanal, acetaldehyde, CO, and  $CO_2$ ). The relative standard error in the conversion and selectivity values were around 5%.

**2.2. Computational Methods.** Density functional theory (DFT) with the PBE (Perdew–Burke–Ernzerhof) functional<sup>23</sup> as implemented in the Vienna Ab Initio Simulation Package (VASP)<sup>24–26</sup> was employed. We added a Hubbard  $U$  term to the PBE functional (DFT +  $U$ ) employing the rotationally invariant formalism by Dudarev et al.,<sup>27</sup> in which only the difference ( $U_{\text{eff}} = U - J$ ) between the Coulomb  $U$  and exchange  $J$  parameters enters. We performed spin-polarized calculations and used the projector augmented wave (PAW) method<sup>28–30</sup> to describe the interaction between the ions and the electrons with the frozen-core approximation.<sup>29</sup> We carried out calculations for  $MgCr_2O_4$  and  $MgCuCr<sub>2</sub>O<sub>4</sub>$  spinel surface models (Figure 1); the energies were corrected for the dipoles present due to the different surface terminations of the model.

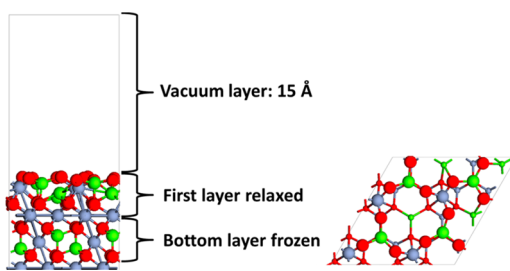


**Figure 1.** Model of the  $MgCr_2O_4(111)$  surface for the DFT calculations (color code: Mg, blue; Cr, green; O, red). For the calculations on the  $MgCuCr_2O_4$ , one out of four Mg atoms in the surface was replaced by Cu.

$MgCr_2O_4$  has the crystal group  $Fd\bar{3}m$  and has 56 atoms per unit cell. Mg and Cr ions occupy the tetrahedral and octahedral sites, respectively. To construct the  $MgCuCr_2O_4$  model, one out of four surface Mg cations in the  $MgCr_2O_4$  model was replaced by Cu. The resulting surface contains Cu and Mg cations in the second layer and O atoms binding to Cu cations in the first layer. The energy cutoff was 400 eV. For Cr, we used the on-site repulsion  $U = 3$  eV, and for the exchange parameter,  $J = 0.9$  eV.<sup>31</sup>

For all of the calculations, the model was a periodic slab with a  $(2 \times 2)$  surface unit cell and lattice constants of  $11.78 \times 11.78$  Å. We verified that the use of the larger  $(2 \times 3)$  super cell had a negligible influence on the results.<sup>32</sup> Because of the relatively large super cell size, a Monckhorst-Pack  $1 \times 1 \times 1$  mesh was used for the Brillouin zone integration. The use of  $k$ -point sampling with a  $2 \times 2 \times 1$  mesh led to negligible energy differences.<sup>32</sup> In the calculations, the bottom layer of the models was kept frozen. The vacuum space above the slab was 15 Å. For the Au cluster model, a bilayer cluster of 10 gold atoms was placed on the (111) surface and then optimized. Some of the gold atoms in the optimized cluster were frozen during subsequent reactivity studies. This approach has been employed before in theoretical studies to simulate reactions at the interface between a metal nanocluster and the subjacent oxide support.<sup>33</sup> Another model consisted of a single Au atom on the  $MgCr_2O_4(111)$  surface.

For calculations involving Au(111) and Au(211) surfaces,  $3 \times 3$  and  $1 \times 3$  unit cells with four metal layers, respectively, were employed. For both models, the top two layers were relaxed and the bottom two layers were frozen to simulate bulk properties. The vacuum thickness was taken as 15 Å. A  $3 \times 3 \times 1$   $k$ -point mesh was employed in the Au slab calculations. Atoms were relaxed until forces were smaller than 0.05 eV·Å<sup>-1</sup>. The location and energy of transition states were calculated with the climbing-image nudged elastic band method.<sup>34</sup> The transition state was identified as the highest energy image with a force tangent to the reaction coordinate and with all atomic forces less than 0.05 eV·Å<sup>-1</sup>. The harmonic vibrational modes were calculated for the transition state image to confirm the occurrence of a single imaginary vibrational frequency.

### 3. RESULTS AND DISCUSSION

**3.1. Characterization.** Figure 2 shows XRD patterns of the  $MgCr_2O_4$  and  $MgCuCr<sub>2</sub>O<sub>4</sub>$  supports and the gold-containing catalysts. The structure of all materials was similar to that of the  $MgCr_2O_4$  spinel reported in the literature.<sup>35</sup> The XRD patterns did not change upon deposition–precipitation of gold and subsequent calcination to obtain gold nanoparticles. The most important physicochemical properties of these materials are collected in Table 2. The BET surface areas of the spinel supports are very low, which is due to the high calcination temperature. Representative TEM images of the two spinel-supported gold catalysts are given in Figure 3. The average particle sizes were  $3.5 \pm 0.9$  nm for Au/ $MgCr_2O_4$  and  $3.2 \pm 0.9$  nm for Au/ $MgCuCr<sub>2</sub>O<sub>4</sub>$ .

**3.2. Catalytic Activity Measurements.** Au/ $MgCuCr<sub>2</sub>O<sub>4</sub>$  oxidized propylene with reasonable activity and good selectivity to acrolein in the presence of  $O_2$ . The main byproducts observed were  $CO_2$ , CO, and acetaldehyde. Figure 4 shows the propylene conversion and acrolein selectivity as a function of temperature for Au/ $MgCuCr<sub>2</sub>O<sub>4</sub>$ . The highest acrolein yield was obtained at 200 °C. At a propylene conversion of 1.6%, the acrolein selectivity was 83%. This selectivity is comparable to

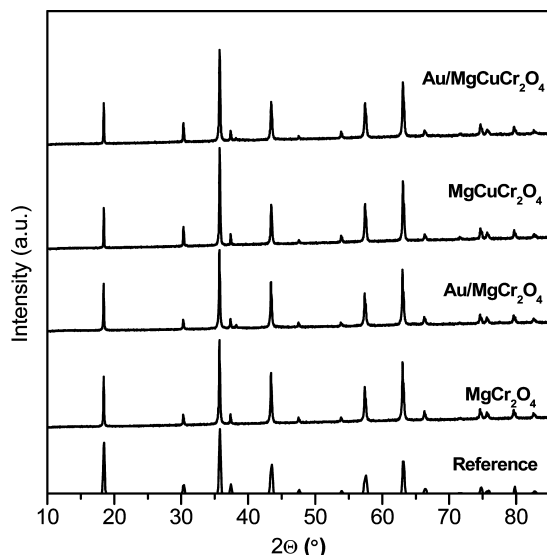


**Figure 2.** XRD patterns of  $\text{MgCr}_2\text{O}_4$ ,  $\text{MgCuCr}_2\text{O}_4$ , and the AuNP-containing catalysts derived from them. The XRD patterns agree with that of the pure  $\text{MgCr}_2\text{O}_4$  spinel phase (JCPDS 10-0351). The reference pattern of  $\text{MgCr}_2\text{O}_4$  is generated from the structural data reported by Kemei et al.<sup>35</sup>

**Table 2. Characterization of the Supports and the Gold Catalysts**

sample	Cu/Mg ratio	$S_{\text{BET}}$ ( $\text{m}^2/\text{g}$ )	[Au] (wt %)	$d_{\text{Au}}$ (nm)
$\text{MgCr}_2\text{O}_4$	0	16		
$\text{Au/MgCr}_2\text{O}_4$	0	n.d.	0.93	$3.5 \pm 0.9$
$\text{MgCuCr}_2\text{O}_4$	0.25	5		
$\text{Au/MgCuCr}_2\text{O}_4$	0.25	n.d.	0.90	$3.2 \pm 0.9$

the value reported by Bracey et al.<sup>1</sup> for a CuAu/SiO<sub>2</sub> catalyst using oxygen as the oxidant. At temperatures above 220 °C, the conversion strongly increased at the expense of the acrolein selectivity. At higher temperatures, the propylene conversion was limited by the amount of O<sub>2</sub> in the feed. CO<sub>2</sub> was the dominant product under these conditions. After evaluating the catalyst performance at different temperatures by gradually increasing the reaction temperature to 300 °C, reaction cycles were performed at decreasing temperatures down to 200 °C. The conversion and selectivity values were exactly the same as the ones obtained during the ramp up of the temperature. This indicates that, even at higher temperatures, the surface of the

catalyst remained unchanged and that there was no extensive sintering of AuNPs or decomposition of the spinel support. For Au/MgCr<sub>2</sub>O<sub>4</sub>, the acrolein selectivities at 200 °C and below were also high, although the propylene conversion was much lower than for Au/MgCuCr<sub>2</sub>O<sub>4</sub>. Different from Au/MgCuCr<sub>2</sub>O<sub>4</sub>, the increase in the reaction temperature did not lead to a sharp increase in the propylene conversion for Au/MgCr<sub>2</sub>O<sub>4</sub>, albeit the acrolein selectivity became very low above 220 °C.

We compared these reaction results with the literature data listed in Table 1. Typically, Cu-only catalysts are active in acrolein formation at relatively high temperatures (~400 °C), whereas gold shows its best performance at much lower temperature. Combining Cu with Au shifted the activity of the Cu catalysts to lower temperatures, as was also shown by Belin et al.<sup>14</sup> These authors obtained an optimum acrolein yield of 8.9% at 320 °C. From the present data, it can be deduced that gold plays an important role in the catalytic mechanism of propylene oxidation to acrolein.

Figure 4 also contains data for the oxidation of propylene over the MgCuCr<sub>2</sub>O<sub>4</sub> support without gold nanoparticles. The propylene conversion below 220 °C was lower than for Au/MgCuCr<sub>2</sub>O<sub>4</sub>. Above 220 °C, the contribution of propylene combustion was evident, and the converted propylene was completely oxidized when the temperature was above 270 °C. Despite the absence of gold, the acrolein selectivity for MgCuCr<sub>2</sub>O<sub>4</sub> is around 60–70% at lower temperatures. In addition to CO<sub>2</sub>, CO, and acetaldehyde, propylene oxide was also observed with a selectivity of 3.5%. Figure 4 also shows that, without Cu, the MgCr<sub>2</sub>O<sub>4</sub> exhibited only a very low acrolein selectivity, below 25%, for all temperatures investigated.

These data suggest that there is significant synergy between Au nanoparticles and Cu of the support in the acrolein formation from propylene oxidation. The presence of gold modifies the reaction pathway of propylene over the MgCuCr<sub>2</sub>O<sub>4</sub> support. It is reasonable to conclude that preferential adsorption of propylene on gold decreases the amount of byproducts formed. Adsorption of propylene on gold has been discussed by Nijhuis et al.,<sup>36</sup> who used X-ray absorption near-edge spectroscopy to determine that propylene is  $\pi$ -bonded to gold. The complete oxidation of propylene at higher temperatures appears to be associated with the presence of Cu in the support.

Recently, the excellent catalytic performance of the same Au/MgCuCr<sub>2</sub>O<sub>4</sub> catalyst in the oxidation of ethanol to acetaldehyde has been attributed to synergy between Au<sup>0</sup> and

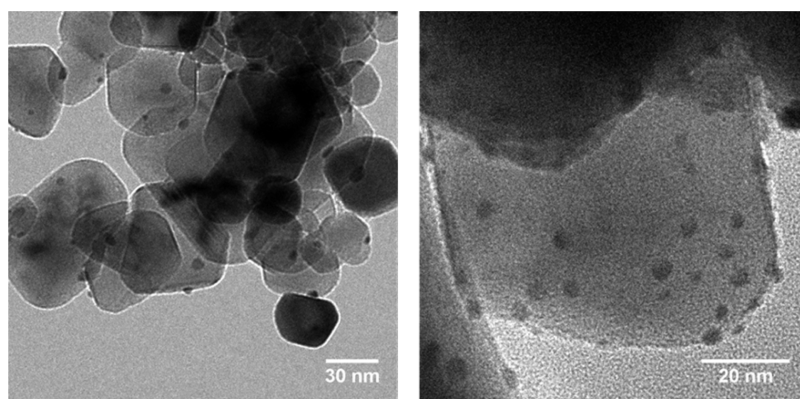


**Figure 3.** Representative TEM images of (left) Au/MgCr<sub>2</sub>O<sub>4</sub> and (right) Au/MgCuCr<sub>2</sub>O<sub>4</sub>.

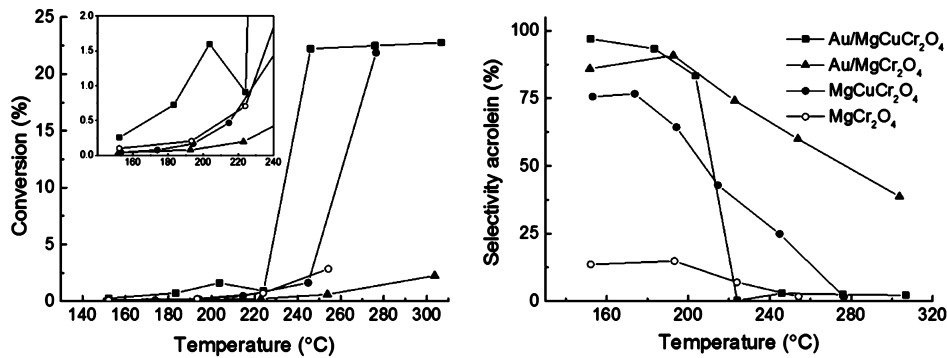


**Figure 4.** Propylene oxidation to acrolein by (■)  $\text{Au/MgCuCr}_2\text{O}_4$ , (▲)  $\text{Au/MgCr}_2\text{O}_4$ , (●)  $\text{MgCuCr}_2\text{O}_4$ , and (○)  $\text{MgCr}_2\text{O}_4$  ( $\text{GHSV} = 10\,000 \text{ mL g}_{\text{cat}}^{-1} \text{ h}^{-1}$ ). (left) Propylene conversion and (right) acrolein selectivity) as a function of temperature.

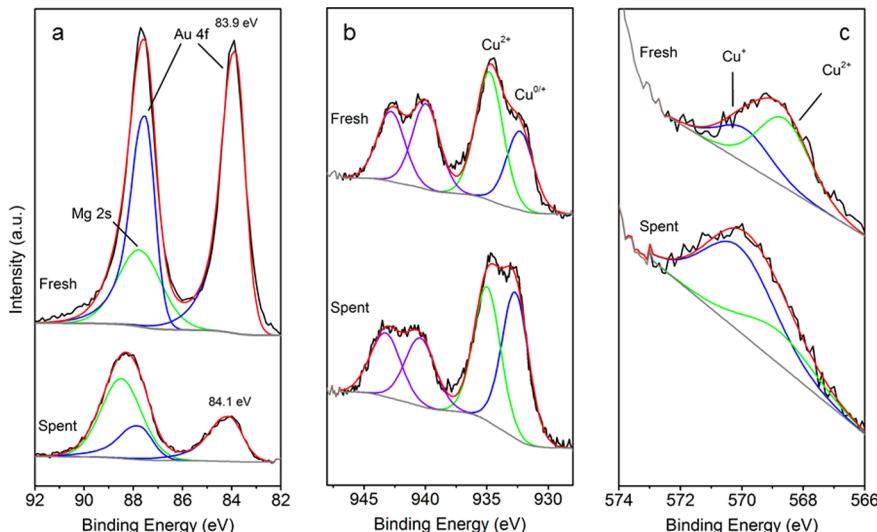


**Figure 5.** XP spectrum of (a) the Au 4f state and (b) the Cu 2p state and (c) the Auger spectrum of the Cu LMM state of (top) fresh and (bottom) spent  $\text{Au/MgCuCr}_2\text{O}_4$  (note the overlap of the Mg 2s state in the Au 4f binding energy range).

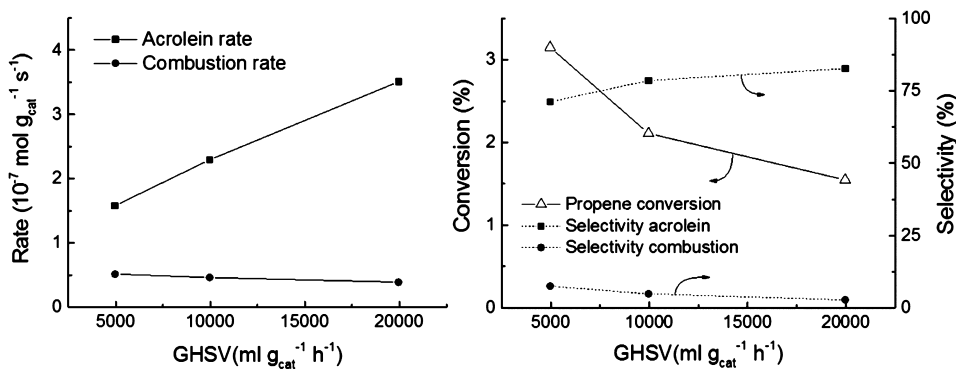


**Figure 6.** Oxidation of propylene with oxygen over  $\text{Au/MgCuCr}_2\text{O}_4$ . (left) Rates of acrolein formation and propylene combustion and (right) conversion of propylene and selectivities to acrolein and combustion products as a function of the GHSV ( $T = 210^\circ\text{C}$ ; feed: 10%  $\text{C}_3\text{H}_6$ , 10%  $\text{O}_2$ ).

$\text{Cu}^+$  surface species.<sup>22</sup> In line with this assertion, the spent  $\text{Au/MgCuCr}_2\text{O}_4$  catalyst (recovered after the activity measurements in Figure 4) contained gold nanoparticles in the metallic state, as evidenced by XPS data (Figure 5). The gold nanoparticles in the fresh sample were also in the metallic state. The surface region of the spent catalyst contained  $\text{Cu}^+$  and  $\text{Cu}^{2+}$  species, as followed from a combination of Cu 2p XP and Cu LMM Auger spectra (Figure 5). The  $\text{Cu}^+$  content was higher in the spent sample than in the fresh sample. The presence of  $\text{Cu}^+$  is in line with the high acrolein selectivity. As

indicated above, acrolein formation in Cu-containing catalysts is usually associated with the presence of  $\text{Cu}^+$ , whereas  $\text{Cu}^{2+}$  mainly catalyzes complete combustion of propylene.<sup>11</sup> Thus, we conclude that there is strong synergy between  $\text{Au}^0$  nanoparticles and  $\text{Cu}^+$  ions in the surface in the oxidation of propylene to acrolein.

The influence of the residence time during propylene oxidation was evaluated by varying the total flow rate and maintaining the same reactant concentrations and amount of catalyst. Conversions as high as 3.2% could be obtained at low

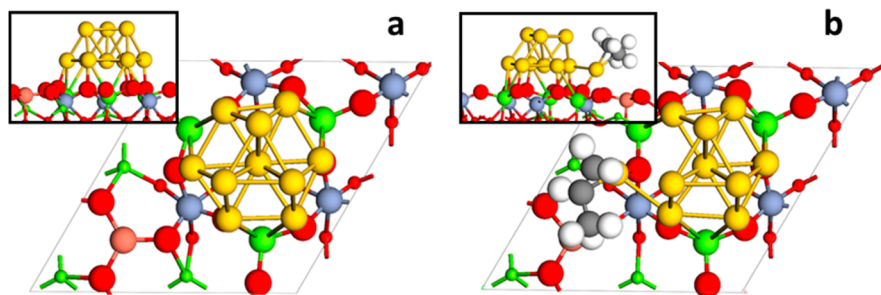


**Figure 7.** (a) Surface model for DFT calculation consisting of a MgCr<sub>2</sub>O<sub>4</sub> spinel with one out of four Mg<sup>2+</sup> ions in the surface replaced by Cu<sup>2+</sup> with on top of it a cluster of 10 gold atoms and (b) optimized structure of propylene adsorbed to a gold atom located at the interface with the support.

space velocities. This led to a small decrease in the acrolein selectivity to 71% at the lowest space velocity. It was seen that more combustion products were formed. As follows from Figure 6, the rate of acrolein formation increased with increasing space velocity, whereas the rate of combustion decreased. We expect that, at higher GHSV, as the reactor starts to operate under true differential conditions, the acrolein formation rate will stabilize and will be independent of the residence time.

In the experiments in which hydrogen was added to the gas feed (10 vol %) together with oxygen and propylene for the oxidation over Au/MgCuCr<sub>2</sub>O<sub>4</sub>, no beneficial effect of hydrogen was observed on the conversion or the selectivity. In line with this, the conversion of hydrogen was very low (<5%). Vaughan et al. also reported that hydrogen cofeeding did not influence the oxidation of propylene over Cu/SiO<sub>2</sub>.<sup>7</sup> Other gold catalysts, however, behave in a different manner. For instance, when hydrogen was added to the propylene/oxygen feed on a Au/SiO<sub>2</sub>, the conversion increased and the acrolein selectivity decreased due to the formation of other carbon-containing byproducts, such as acetone and propanal. A possible mechanism is that OOH intermediates dissociate, producing water and reactive O adatoms that can attack the allylic bond of propylene, resulting in a variety of products, including acrolein. Bracey et al. reported that the addition of hydrogen in the feed favored the formation of acrolein for CuAu/SiO<sub>2</sub>.<sup>1</sup> These authors postulated that the presence of hydrogen increased the amount of oxidizing species through the formation of OOH species that may react directly or indirectly oxidize with propylene. The formation of OOH over CuAu/SiO<sub>2</sub> is related to the presence of gold.<sup>7</sup> The finding that Au/MgCuCr<sub>2</sub>O<sub>4</sub> behaves very differently indicates that the consumption of oxygen is faster in the direct oxidation reaction to acrolein over the Au–Cu interface than the rate at which OOH species are formed with hydrogen over the gold nanoparticles. The alternative explanation is that there is another more favorable adsorption site for O<sub>2</sub>.

When the MgCuCr<sub>2</sub>O<sub>4</sub> was used in a propylene/O<sub>2</sub>/H<sub>2</sub> mixture, the reaction proceeded with high selectivity (90%) to propane at 1.4% propylene conversion. Similar to the reaction with oxygen only, the conversion at 270 °C increased to 16%, mainly as a result of combustion of propylene. The fact that when Au is deposited on the Cu-containing spinel no significant hydrogenation of propene is observed might be due to deposition of Au NPs over the sites responsible for the hydrogenation.

The use of copper catalysts for the hydrogenation of propylene and ethylene was demonstrated at the beginning of the 20th century.<sup>37,38</sup> Sussman et al. performed a kinetic study

on the hydrogenation of propylene over copper–magnesia catalyst,<sup>39</sup> in which a dual site reaction mechanism was proposed between atomically adsorbed hydrogen and propylene. The hydrogenation over Au depends on the particle size, and it has been argued that it becomes more dominant as the gold becomes more finely dispersed.<sup>40</sup> Evidently, the particles in the present Au/MgCuCr<sub>2</sub>O<sub>4</sub> catalyst were too large to catalyze the hydrogenation reaction. On the other hand, the catalyst with AuNP deposited on the copper-free support (Au/MgCr<sub>2</sub>O<sub>4</sub>) produced acetone in a nearly similar amount as acrolein. The conversion of propylene remained low. This can be understood by the formation of OOH species over the gold nanoparticles, similar to CuAu/SiO<sub>2</sub>.<sup>1</sup> In the absence of Cu, oxygen can react with hydrogen over AuNP and, as explained before, release water and an active O adatom. This O adatom can react with propylene in a variety of manners. We also found that, at high temperatures, the conversion of hydrogen was complete.

N<sub>2</sub>O can be better for selective oxidation reactions than molecular oxygen because the N–O bond in N<sub>2</sub>O is weaker than the O–O bond in O<sub>2</sub> and also because there is only one oxygen atom per oxidant molecule.<sup>41</sup> Accordingly, its use as a mild oxidant for propylene oxidation has been widely explored. For instance, propylene conversions in the 6–12% range with PO selectivities of 40–60% have been reported for silica-supported iron oxide. Llorca et al.<sup>16</sup> obtained for CuAu/TiO<sub>2</sub> propylene conversions of 2.5% with PO selectivities up to 50%. In the present study, we found that oxidation of propylene with N<sub>2</sub>O over Au/MgCuCr<sub>2</sub>O<sub>4</sub> resulted in a very low conversion (<0.2%), even though the selectivity to acrolein remained close to 90%. The reason is that the rate of N<sub>2</sub>O dissociation is very low on this catalyst. The conversion of a N<sub>2</sub>O/He feed without propylene was 1% at 200 °C and 2% conversion at 300 °C. The discrepancy between our results and those of Llorca et al.<sup>16</sup> may be due to the oxidation state of Cu in the catalyst support. As explained by Vaughan et al.,<sup>7</sup> metallic copper (Cu<sup>0</sup>) was present in the catalyst, which catalyzes the epoxidation of propylene. According to the XPS analysis of Au/MgCuCr<sub>2</sub>O<sub>4</sub>, the spinel contains Cu<sup>+</sup>, which is argued to be active for the partial oxidation to acrolein.<sup>11</sup>

### 3.2. Computational Modeling. Adsorption of Propylene.

Figure 7a shows the surface model containing a gold cluster used in our DFT calculations. We first examined possible adsorption sites of propylene on the gold cluster. Two adsorption sites were identified: (i) Au atoms that have only other Au atoms as neighbors, and (ii) Au atoms that are neighbored by both Au atoms and support O atoms. We use the expression *interfacial site* for the ensemble of atoms around the latter adsorption site. The adsorption strength of propylene

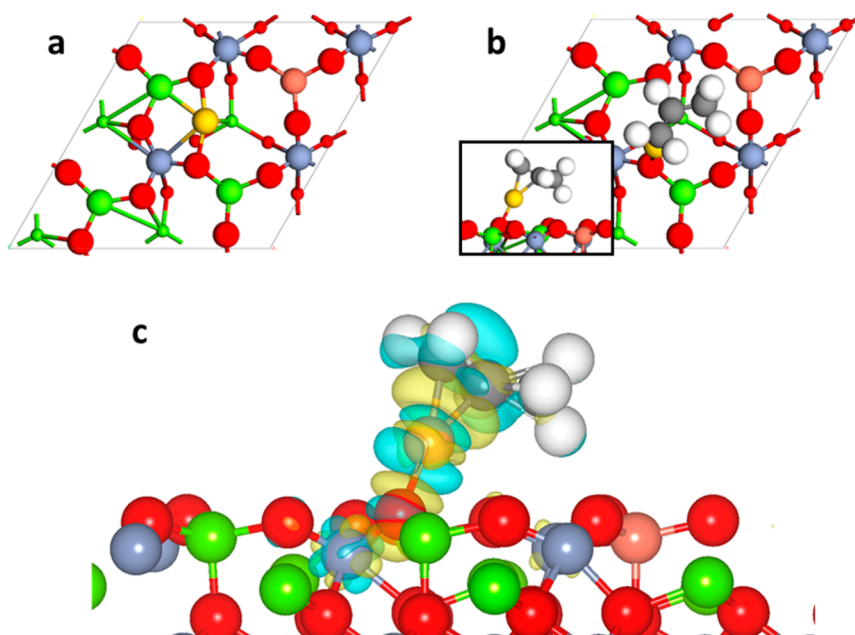


**Figure 8.** (a) Optimized structure of a single Au atom on MgCuCr<sub>2</sub>O<sub>4</sub>, (b) most stable adsorption geometry of propylene on Au<sub>1</sub>/MgCuCr<sub>2</sub>O<sub>4</sub>, and (c) electron density redistribution due to propylene adsorption (blue indicates a decrease in the electron density; yellow, an increase in electron density).

on the first adsorption site is 74 kJ/mol. Propylene is  $\pi$ -bonded on a single Au atom. Adsorption of propylene to one of the interfacial Au atoms resulted in almost complete dissociation of the interfacial Au atom from the Au<sub>10</sub> cluster. This process occurred spontaneously during geometry optimization. In the final stable state (Figure 7b), the distance of the migrated Au atom to its neighbors is much longer than in the initial state. One Au atom is located at a distance of about 3.0 Å, whereas the others are located at distances longer than 5 Å. The initial Au–Au distance in the Au<sub>10</sub> cluster is  $\sim$ 2.8 Å.

To understand better this adsorbate-induced reconstruction of the Au<sub>10</sub> cluster, we computed the cohesive energy of the supported Au<sub>10</sub> cluster in the following manner:  $E_{\text{cohesive}} = E(\text{Au}_{10}/\text{MgCuCr}_2\text{O}_4) + E(\text{MgCuCr}_2\text{O}_4) - E(\text{Au}_9/\text{MgCuCr}_2\text{O}_4) - E(\text{Au}_1/\text{MgCuCr}_2\text{O}_4)$ . This energy is a measure for the energy cost to remove one Au atom from the supported Au cluster. Its value is +48 kJ/mol. The adsorption energy of propylene on a single Au atom on MgCuCr<sub>2</sub>O<sub>4</sub> (Au<sub>1</sub>/MgCuCr<sub>2</sub>O<sub>4</sub>) is 116 kJ/mol. Thus, the overall process of adsorption of propylene on an interfacial Au atom followed by complete dissociation of the propylene–Au adduct from the cluster is favorable by 68 kJ/mol. Note it is comparable to the adsorption energy of propylene on a metallic site of the gold cluster. We then considered whether it would be favorable to remove a gold atom from a large nanoparticle by propylene adsorption and stabilize it on the MgCuCr<sub>2</sub>O<sub>4</sub> support.

For this purpose, we compared the energy of propylene adsorbed on Au<sub>1</sub>/MgCuCr<sub>2</sub>O<sub>4</sub> with the sum of the energies of gas-phase propylene, a single Au atom in bulk gold, and the MgCuCr<sub>2</sub>O<sub>4</sub> support. The formation energy of propylene adsorbed on a single supported gold atom is exothermic by 28 kJ/mol. Accordingly, we infer that strong propylene adsorption to gold atoms can lead to the reconstruction of gold nanoparticles and formation of isolated gold atoms. Although such a process will involve significant kinetic barriers for large gold clusters and nanoparticles, our data show that the interfacial Au atoms of a small cluster can almost completely

dissociate from this cluster without significant barrier upon interaction with propylene. Experimentally, such behavior has not yet been reported; however, we suggest that the changes noted in the Au L<sub>3</sub> edge structure upon propylene adsorption to Au/SiO<sub>2</sub> catalysts as reported by Nijhuis et al.<sup>36</sup> may be related to adsorption-induced restructuring of gold clusters on the silica-supported catalyst.

**Reaction Mechanism on Au<sub>1</sub>/MgCuCr<sub>2</sub>O<sub>4</sub>.** We considered propylene adsorbed to a single Au atom on the MgCuCr<sub>2</sub>O<sub>4</sub> support as a model for investigating propylene oxidation. For some reaction steps, we also investigated the energetics for the Au<sub>1</sub>/MgCr<sub>2</sub>O<sub>4</sub> model to evaluate the role of Cu. The Au<sub>1</sub>/MgCuCr<sub>2</sub>O<sub>4</sub> model is shown in Figure 8a. Other less-stable locations of an isolated Au atom on the MgCuCr<sub>2</sub>O<sub>4</sub> surface are given in the Supporting Information. Bader charge analysis of the most stable configuration shows that the gold atom is positively charged as a result of the interaction with the support (+0.25e). The spin magnetic moment of the gold atom with a size of 0.25 $\mu$  is localized in the Au 5d orbital. The Au-support interaction involves hybridization of the 5d orbital of Au with 2p orbitals of the O atoms of the support. The adsorption energy of propylene on this model is 116 kJ/mol. The adsorption energy of propylene on Au<sub>1</sub>/MgCr<sub>2</sub>O<sub>4</sub> is comparable at 126 kJ/mol. Adsorption of propylene resulted in the migration of the Au atom from its initial bridging position between two oxygen atoms of the support to the top position (Figure 8b). The bonding situation was investigated in more detail by plotting the electron density difference of the adsorbed state and similar states in which either the Au<sub>1</sub>/MgCuCr<sub>2</sub>O<sub>4</sub> or propylene was removed (Figure 8c). The result clearly shows that the  $\pi$ -cloud electron density in propylene is redistributed to the region between the positively charged Au atom and propylene. This strong binding is possible because of the positive charge of the Au atom. The figure shows that the Cr cation is also involved in the bonding. Bader charge analysis confirms that the charge of propylene increases from +0.03e in the gas phase to +0.35e.

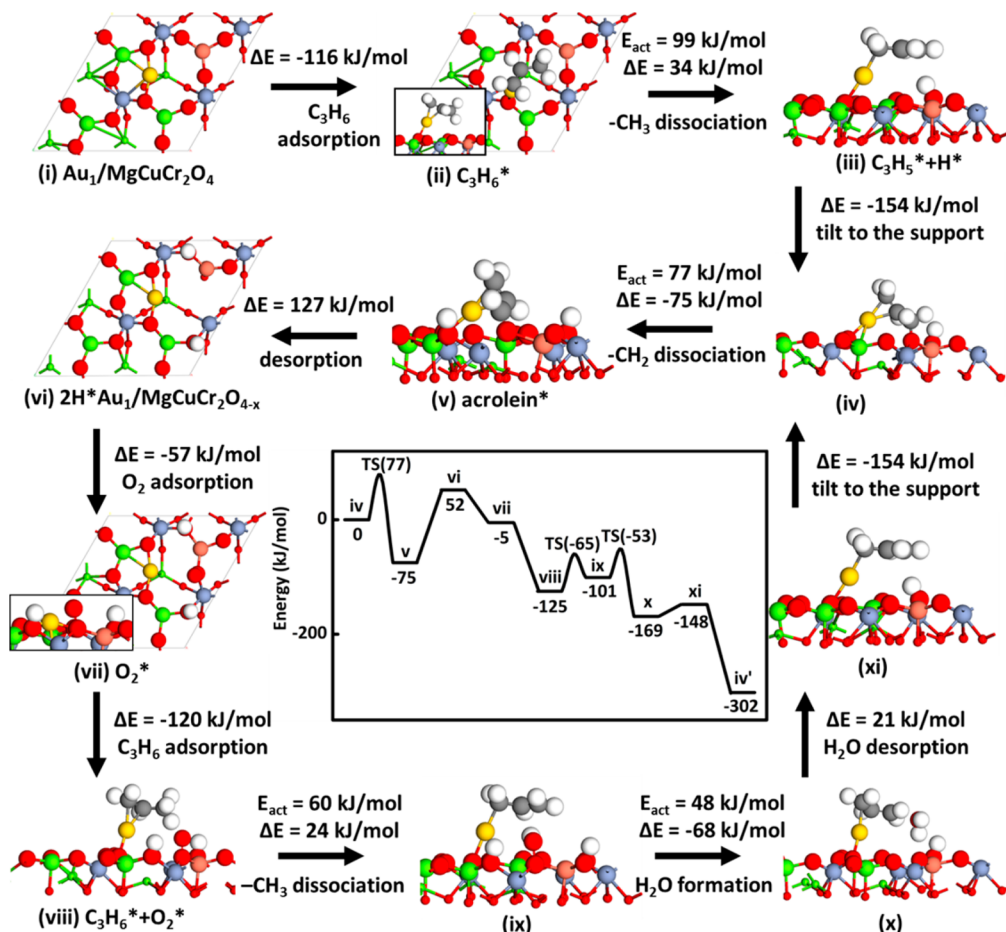


**Figure 9.** Complete reaction energy diagram (middle) with elementary reaction steps for the oxidation of propylene to acrolein on the  $\text{Au}_1/\text{MgCuCr}_2\text{O}_4$  model.

The propylene adsorption energy of 116 kJ/mol for  $\text{Au}_1/\text{MgCuCr}_2\text{O}_4$  is higher than values of 74 kJ/mol for  $\text{Au}_{10}/\text{MgCuCr}_2\text{O}_4$ , 44 kJ/mol for  $\text{Au}(211)$ , and 15 kJ/mol for  $\text{Au}(111)$ . The computed Bader charges for propylene using these surface models are, respectively, +0.35e, +0.17e, +0.14e, and +0.05e; therefore, we conclude that the adsorption energy strongly correlates with the oxidation state of the Au atom. Although we did not investigate in detail the charge on the Au atoms in the  $\text{Au}_{10}/\text{MgCuCr}_2\text{O}_4$  model, we speculate that the Au atom on the top of the  $\text{Au}_{10}$  cluster is also slightly charged due to the proximity of the support. The driving force for dissociation of the Au atom at the interface from the cluster upon propylene adsorption is the gain in hybridization energy between the  $\pi$ -orbitals of propylene and the increasingly empty d orbitals of Au interacting more strongly with the support.

Figure 9 shows the complete reaction diagram based on our calculations, including important intermediate structures for the oxidation of propylene to acrolein. One of the allylic C–H bonds in adsorbed propylene (state ii, Figure 9) dissociates with the H atom relocating to one of the oxygen anions of the support. These O atom are coordinated to both Cu and Cr cations (state iii). The activation barrier for this step is 99 kJ/mol, and the C–H dissociation step is endothermic by 34 kJ/mol. In the transition state, the C–H bond distance is increased from its initial value of 1.10 to 1.44 Å. The bond distance in the transition state between O and H is 1.19 Å. When this reaction step was carried out for  $\text{Au}_1/\text{MgCr}_2\text{O}_4$ , the energy change was the same, indicating that the basicity of the surface O atoms is

the same, in line with our earlier findings for ethanol oxidation.<sup>32</sup> We also investigated the same allylic C–H bond dissociation step for propylene adsorbed on  $\text{Au}_{10}/\text{MgCuCr}_2\text{O}_4$ , which is on the gold site on top of the cluster. In this case, the dissociation takes place on the gold cluster without the aid of the O atoms of the support because they are too distant. The reaction energy of 119 kJ/mol is much larger than the reaction energy for propylene adsorbed to a single Au atom ( $\Delta E = 34$  kJ/mol). This result confirms that the first step of C–H bond dissociation in the  $\text{CH}_3$  moiety is catalyzed by support O atoms.

Following C–H bond cleavage, the adsorption mode of the remaining  $\text{C}_3\text{H}_5$  allyl intermediate changes. The allyl is bound via the terminal C atom to the Au atom with a bond distance of 2.06 Å. The other two C atoms form a new double bond so that effectively, a  $\text{Au}–\text{CH}_2–\text{CH}=\text{CH}_2$  intermediate is formed. This structure can tilt to one of the other support O atoms with negligible barrier, resulting in a  $\text{Au}–\text{CH}_2–\text{CH}–\text{CH}_2–\text{O}_{\text{support}}$  intermediate in which the middle C atom again binds to the Au atom (state iv). This adsorption state is 154 kJ/mol more stable than state iii.

From this configuration, one of the C–H bonds of the  $\text{CH}_2$  group, which is bound to the support O anion, dissociates to a neighboring O atom of the support (state v). The activation barrier for this step is 77 kJ/mol. The formation of adsorbed acrolein is thermodynamically favorable ( $\Delta E = -75$  kJ/mol). Adsorbed acrolein is adsorbed 2-fold, namely, with its  $\text{CH}_2$  group coordinating to the Au atom and the oxygen atom of its

carbonyl group bridging between Cu and Mg. The Au–C and Cu–O distances in the adsorbed complex are 2.19 and 2.34 Å, respectively. Desorption of acrolein, which costs 127 kJ/mol, generates one surface oxygen vacancy on the support (state vi). We found that acrolein desorption from the  $\text{Au}_1/\text{MgCr}_2\text{O}_4$  model is more difficult than the desorption from the  $\text{Au}_1/\text{MgCuCr}_2\text{O}_4$  model ( $\Delta E_{\text{des}} = 159 \text{ kJ/mol}$ ). This is because the Mg–O bond is stronger than the Cu–O bond. Thus, we argue that the lower catalytic performance of  $\text{Au}/\text{MgCr}_2\text{O}_4$  compared with  $\text{Au}/\text{MgCuCr}_2\text{O}_4$  is due to slower desorption of the acrolein product.

The other half cycle of the mechanism starts by the adsorption of propylene on the gold atom. Molecular oxygen adsorbs to the oxygen vacancy with an energy of 57 kJ/mol (state viii). The O–O bond distance is elongated from its gas phase value of 1.23 to 1.32 Å in the adsorbed complex. This points to the formation of a peroxide-type  $\text{O}_2^-$  species. The activation of the allylic C–H bond results in a hydroperoxy (OOH) species (state ix). The barrier for this oxidation step of 60 kJ/mol is lower than the barrier for C–H bond activation involving the oxygen anion of  $\text{MgCuCr}_2\text{O}_4$ . The reaction resulting in OOH is endothermic by 24 kJ/mol. The OOH group reacts with one of the nearby OH groups and forms weakly adsorbed water ( $\text{OOH}^* + \text{OH}^* \rightarrow \text{O}^* \cdots \text{H}_2\text{O} + \text{O}^*$ ) with an activation barrier of only 48 kJ/mol and a reaction energy of –68 kJ/mol. Desorption of water costs 21 kJ/mol. Similar to the reaction steps discussed above, the resulting  $\text{CH}_2-\text{CH}-\text{CH}_2$  intermediate bound to the gold atom tilts to the support surface and cleaves another of the  $\text{CH}_2$  C–H bonds to form adsorbed acrolein (state iv). This step is followed by desorption of acrolein. The catalytic cycle will now proceed by adsorption of oxygen and propylene so that structure iv is the recurring main reaction intermediate that leads to acrolein formation. On the clean surface, an oxygen atom of the  $\text{MgCuCr}_2\text{O}_4$  support will oxidize the allylic C–H bond with an activation barrier of 99 kJ/mol. After its removal, the catalytic cycle will proceed by allylic C–H bond activation with adsorbed  $\text{O}_2$ , which has a lower activation barrier of 60 kJ/mol.

To relate these data better to the experimental observations, we determined the oxidation state of Cu by a Bader charge analysis for the states along the proposed reaction mechanism for acrolein formation. The results are collected in Table 3. The oxidation state of Cu is close to unity in all cases. The most significant change is seen in the acrolein desorption step. This

step involves the cleavage of the Cu–O bond. The coordination number of Cu changes from 4 to 3, which explains the decrease of the negative charge. These results are in accordance with the experimental XPS data and, accordingly, support the proposed mechanism. Below, we will discuss in more detail the role of Cu in the mechanism.

We argue that the presence of  $\text{O}_2$  in the gas phase avoids further reduction of Cu species to the extent that Cu may be reduced to the metallic state and, possibly, Cu sinters. It is worthwhile to refer to oxygen-induced self-healing of CuRh alloys.<sup>42</sup> In that work,  $\text{H}_2$  production by  $\text{CuRhO}_2$  in Ar-saturated solution was unstable as a result of formation of metallic Cu; in the presence of  $\text{O}_2$ ,  $\text{CuRhO}_2$  remains active because the reduction process is prevented.

**Epoxidation of Adsorbed Propylene.** The reaction mechanism discussed for the formation of acrolein involves a hydroperoxide surface intermediate. Because this intermediate is considered an essential intermediate in the epoxidation of propylene to propylene oxide, we also explored the possibility of propylene oxide formation. It requires the reaction of the double bond of propylene with an O species instead of dissociation of one of its allylic C–H bonds. We examined four possible paths that lead to propylene oxide (Figure 10). The first three paths are catalyzed by  $\text{O}^*$ ,  $\text{O}_2^*$ , and  $\text{OOH}^*$  species via Langmuir–Hinshelwood type mechanisms, and the fourth one is catalyzed by  $\text{O}^*$  (Figure 10d) via an Eley–Rideal type mechanism with propylene reacting from the gas phase. The first path starts by migration of the initially gold  $\pi$ -bonded propylene to a support oxygen atom, forming an oxometalacycle (OMC) intermediate, with one of the C atoms of propylene  $\sigma$ -binding to the Au atom and another one binding to a support O atom. The OMC intermediate is the well-established precursor for the epoxidation of propylene.<sup>8,43</sup> A similar structure has been proposed in propylene epoxidation catalyzed by silver oxide.<sup>44</sup> The OMC intermediate is less stable than the initial adsorption state by 28 kJ/mol.

The epoxidation proceeds as follows: First, the Au–C bond is broken, forming a metastable state that is less stable by 122 kJ/mol, then the middle C atom coordinates to the O atom to form propylene oxide. This state is more stable by 87 kJ/mol than the metastable structure. Desorption of propylene oxide costs 68 kJ/mol. The two key steps in the process are the cleavage of the Au–C bond and the formation of the second C–O bond. The total energy required to form the metastable state from the initial adsorption state is 150 kJ/mol. The energy cost is higher than the C–H bond cleavage in the methyl group by surface O ( $E_{\text{act}} = 99 \text{ kJ/mol}$ ,  $\Delta E = 34 \text{ kJ/mol}$ ) and by adsorbed  $\text{O}_2$  ( $E_{\text{act}} = 99 \text{ kJ/mol}$ ). Thus, acrolein formation is preferred over propylene oxide formation.

The same conclusion can be drawn when epoxidation involving adsorbed  $\text{O}_2$  is considered (Figure 10b): strong adsorption between propylene and Au inhibits the epoxidation step. The epoxidation process catalyzed by the adsorbed OOH surface intermediate proceeds by the dissociation of the  $\text{OOH}^*$  group to form the OMC intermediate. This reaction step has a barrier of 155 kJ/mol and an exothermic reaction energy of 118 kJ/mol. Similar to the pathways in Figure 10a,b, it costs considerable energy—in this case, 210 kJ/mol—for the OMC intermediate to form the metastable state that precedes epoxidation. These energetics show that none of the three candidate oxidizing species ( $\text{O}$ ,  $\text{O}_2$ , and  $\text{OOH}$ ) can be involved in the epoxidation of adsorbed propylene, essentially because it requires the cleavage of the strong Au– $\text{C}_3\text{H}_6$  bond. This agrees

**Table 3. Calculated Bader Charges of Cu for Selected States along the Reaction Path for Acrolein Formation on  $\text{Au}_1/\text{MgCuCr}_2\text{O}_4$ <sup>a</sup>**

state	Bader charge ( $e$ )
(i) $\text{Au}_1/\text{MgCuCr}_2\text{O}_4$	+1.02
(ii) $\text{C}_3\text{H}_6^*$	+1.01
(iii) $\text{C}_3\text{H}_5^* + \text{H}^*$	+1.00
(iv)	+0.94
(v) acrolein <sup>*</sup>	+0.91
(vi) $2\text{H}^*\text{Au}_1/\text{MgCuCr}_2\text{O}_{4-x}$	+0.84
(vii) $\text{O}_2^*$	+0.97
(viii) $\text{C}_3\text{H}_6^* + \text{O}_2^*$	+0.97
(ix)	+0.98
(x)	+0.98

<sup>a</sup>The number of the states corresponds to the states in Figure 9.

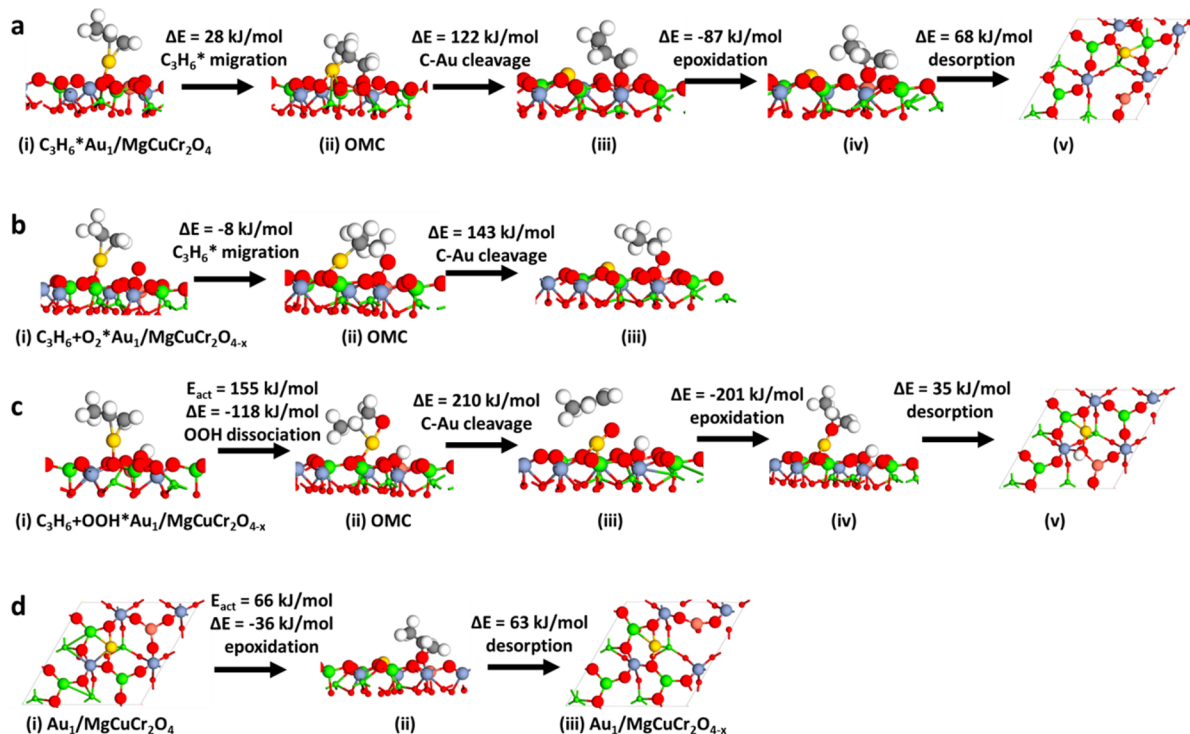


**Figure 10.** Reactions pathways leading to the formation of propylene epoxide via (a) adsorbed O, (b) adsorbed  $\text{O}_2$ , (c) adsorbed OOH, and (d) direct epoxide formation in an Eley–Rideal type mechanism.

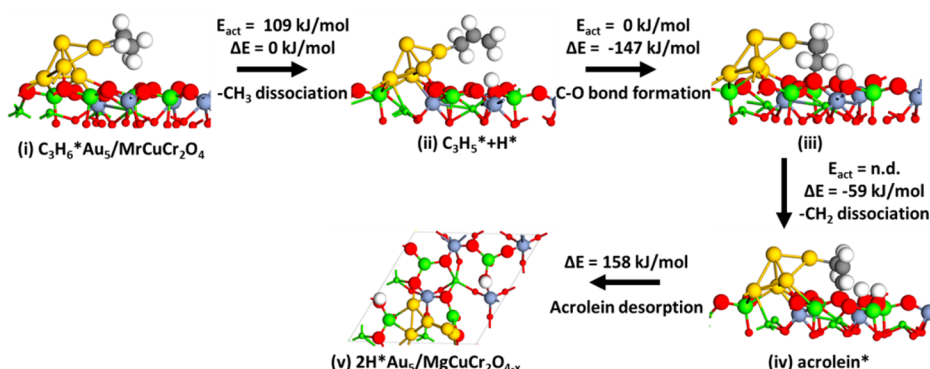


**Figure 11.** Most important reaction steps for the oxidation of adsorbed propylene with a surface O atom of the support to form acrolein in the gas phase. The model is a  $\text{Au}_5$  cluster on the  $\text{MgCuCr}_2\text{O}_4$  support.

with the general notion that Ti is needed to epoxidize propylene.<sup>2</sup> The alternative allylic C–H bond activation that leads to acrolein is more facile. The direct interaction of the double bond in gas phase propylene with the surface O atom via an Eley–Rideal mechanism was also examined (Figure 10d). This reaction step has an activation barrier of 66 kJ/mol and an exothermic reaction energy of 36 kJ/mol. In the transition state, the bond distance between the O atom and the C atoms is 1.87 Å, whereas the Cu–O and Cr–O distances are elongated by 0.1 and 0.14 Å, respectively. It takes 63 kJ/mol to desorb propylene oxide into the gas phase. Although the barrier of this reaction path is not unfavorable, the reaction rate will be low. The reason is that the involvement of a direct propylene adsorption step in this Eley–Rideal mechanism will result in a very low pre-exponential factor.

**Influence of Gold Nuclearity.** In the above, we have shown that the strong interaction between the double bond of propylene and Au can stabilize a single Au atom. This single Au

atom can catalyze with low overall reaction barrier the selective oxidation of propylene to acrolein with molecular oxygen. There is currently no direct experimental evidence for the formation of isolated Au atoms from a cluster or nanoparticle upon propylene adsorption. The TEM images indicate that gold is present predominantly in the nanoparticulate form. On the basis of our computational findings, we speculate that surface reconstruction of the gold atoms at the interface between a gold particle and the support upon propylene adsorption might lead to isolated Au atoms. This was found for the  $\text{Au}_{10}$  model used in our initial modeling efforts. We surmise, however, that similar oxidation chemistry should be possible on gold atoms at the interface between a gold cluster or nanoparticle and the  $\text{MgCuCr}_2\text{O}_4$  support without the isolation of the gold atom to which propylene binds. Therefore, we examined some of the key steps in the proposed reaction mechanism for propylene oxidation to acrolein based on a  $\text{Au}_5$  cluster model.

Because of the different geometry of this cluster compared with the  $\text{Au}_{10}$  bilayer, adsorption of propylene on one of the interface Au atoms does not lead to decomposition of the cluster. The key steps that we examined in this study were (i) allylic C–H activation of adsorbed propylene by an O atom of the support, (ii) the C=O bond formation step, (iii) the C–H bond activation step in adsorbed  $\text{CH}_2\text{—CH}_2\text{—CHO}$  by an O atom of the support, and (iv) acrolein desorption. These steps constitute the most important reaction steps for the reaction of propylene to acrolein. The reaction energetics and the key intermediate structures related to these steps are collected in Figure 11. The energetics for the  $\text{Au}_1$  and  $\text{Au}_5$  models on  $\text{MgCuCr}_2\text{O}_4$  are compared in Table 4. The energy values for

**Table 4. Comparison of Computed Reaction Energies ( $\Delta E$ ) and Activation Barriers ( $E_{\text{act}}$ ) for Selected Key Elementary Reaction Steps in the Oxidation of Propylene to Acrolein for  $\text{Au}_1$  and  $\text{Au}$  Cluster Models Supported on the  $\text{MgCuCr}_2\text{O}_4$  Support<sup>a</sup>**

reaction step	$\text{Au}_1$	Au cluster
allylic C–H oxidation	$E_{\text{act}} = 99$	$E_{\text{act}} = 109$
C–O bond formation	$\Delta E = 154$	$\Delta E = 147$
C–H ( $\text{CH}_2$ ) oxidation	$\Delta E = -75$	$\Delta E = -59$
acrolein desorption	$\Delta E = 159$	$\Delta E = 158$

<sup>a</sup>All energies are in kJ/mol.

both models are very comparable, indicating that the reaction mechanism explored in detail for  $\text{Au}_1/\text{MgCuCr}_2\text{O}_4$  for propylene oxidation to acrolein may also be expected to be relevant for a larger Au cluster on the same support. This conclusion is not surprising because the main role of Au is to provide an adsorption site for propylene and the various reaction intermediates. The C–H bond activation reactions are catalyzed by surface O atoms of the support, and the formation of the C–O bond and the desorption of acrolein relate to the metal–O bond strength. Thus, we argue that gold atoms, clusters, and nanoparticles can all catalyze acrolein formation from propylene. For gold nanoparticles, we expect that the activity will increase with an increasing perimeter between the gold particles and the support.

#### 4. CONCLUSIONS

The present study showed that Au nanoparticles supported on  $\text{MgCuCr}_2\text{O}_4$  can catalyze the aerobic oxidation of propylene to acrolein. At a temperature of 200 °C, the acrolein selectivity was 83% at a propylene conversion of 1.6%. The bifunctional Au–Cu catalyst was more active and selective than  $\text{MgCuCr}_2\text{O}_4$  and  $\text{Au}/\text{MgCr}_2\text{O}_4$ . This catalyst provides catalytic performance comparable to that of earlier investigated bimetallic AuCu catalysts. The experimental data point to strong synergy between metallic gold nanoparticles and Cu<sup>+</sup> sites of the support. Hydrogen affected neither the rate of acrolein formation nor the selectivity. When O<sub>2</sub> was replaced by N<sub>2</sub>O as the oxidant, the catalytic performance was very poor.

Quantum-chemical modeling identified reaction mechanisms for the conversion of propylene into acrolein with molecular oxygen involving gold atoms and the  $\text{MgCuCr}_2\text{O}_4$  support. Propylene strongly adsorbs to Au. For a small  $\text{Au}_{10}$  cluster, propylene adsorption on one of the interfacial gold atoms led to the dissociation of this Au atom from the initial Au cluster. The catalytic reaction on such an isolated Au atom involves allylic C–H oxidation by adsorbed O<sub>2</sub>. The resulting OOH

species forms H<sub>2</sub>O with another H atom and an intermediate  $\text{CH}_2\text{—CH—CH}_2$  that is bound to the gold atom and a surface O atom. Acrolein is obtained by oxidation of one of the C–H bonds of the  $\text{CH}_2$  group bound to the surface O atom. Desorption of acrolein is the most difficult step. Cu is essential in the mechanism to facilitate acrolein desorption. Without Cu, the desorption energy is much higher because the Mg–O bond is much stronger than the Cu–O bond. It explains the experimentally observed lower reaction rate for  $\text{Au}/\text{MgCr}_2\text{O}_4$ . The computational data also show that dissociation of the Au atom from its initial cluster is not essential for the reaction mechanism. Gold provides an adsorption site for propylene via its π-bond, and the basic oxygen atoms of the support facilitate the two H abstraction reactions.

#### ■ ASSOCIATED CONTENT

##### S Supporting Information

The following file is available free of charge on the ACS Publications website at DOI: 10.1021/cs5017062

Figure showing other stable adsorption sites of single Au on  $\text{MgCr}_2\text{O}_4(111)$  surface (PDF)

#### ■ AUTHOR INFORMATION

##### Corresponding Author

\*E-mail: e.j.m.hensen@tue.nl.

##### Present Address

<sup>§</sup>(Peng Liu) Huazhong University of Science and Technology, Wuhan, People's Republic of China.

##### Notes

The authors declare no competing financial interest.

#### ■ REFERENCES

- Bracey, C. L.; Carley, A. F.; Edwards, J. K.; Ellis, P. R.; Hutchings, G. J. *Catal. Sci. Technol.* **2011**, *1*, 76–85.
- Nijhuis, T. A.; Makkee, M.; Moulijn, J. A.; Weckhuysen, B. M. *Ind. Eng. Chem. Res.* **2006**, *45*, 3447–3459.
- Callahan, J. L.; Szabo, J. J.; Berthold, G. U.S. Patent US3186955 A, 1965.
- Adams, M. L.; Hearne, G. W. U.S. Patent US2451485 A, 1948.
- Adams, C. R.; Jennings, T. J. *J. Catal.* **1964**, *3*, 549–558.
- Su, W.; Wang, S.; Ying, P.; Feng, Z.; Li, C. *J. Catal.* **2009**, *268*, 165–174.
- Vaughan, O. P. H.; Kyriakou, G.; Macleod, N.; Tikhov, M.; Lambert, R. M. *J. Catal.* **2005**, *236*, 401–404.
- Torres, D.; Lopez, N.; Illas, F.; Lambert, R. M. *J. Am. Chem. Soc.* **2005**, *127*, 10774–10775.
- Torres, D.; Lopez, N.; Illas, F.; Lambert, R. M. *Angew. Chem., Int. Ed.* **2007**, *46*, 2055–2058.
- Tuysuz, H.; Galilea, J. L.; Schuth, F. *Catal. Lett.* **2009**, *131*, 49–53.
- Reitz, J. B.; Solomon, E. I. *J. Am. Chem. Soc.* **1998**, *120*, 11467–11478.
- Monnier, J. R.; Hartley, G. W. *J. Catal.* **2001**, *203*, 253–256.
- Holbrook, L. L.; Wise, H. *J. Catal.* **1971**, *20*, 367–373.
- Belin, S.; Bracey, C. J.; Briois, V.; Ellis, P. R.; Hutchings, G. J.; Hyde, T. I.; Sankar, G. *Catal. Sci. Technol.* **2013**, *3*, 2944–2957.
- Sinfelt, J. H.; Barnett, A. E. U.S Patent US3989674 A, 1976.
- Llorca, J.; Dominguez, M.; Ledesma, C.; Chimentao, R. J.; Medina, F.; Sueiras, J.; Angurell, I.; Seco, M.; Rossell, O. J. *Catal.* **2008**, *258*, 187–198.
- Cant, N. W.; Hall, W. K. *J. Phys. Chem. A* **1971**, *75*, 2914–2921.
- Gasior, M.; Grzybowska, B.; Samson, K.; Ruszel, A.; Haber, J. *Catal. Today* **2004**, *91*, 131–135.
- Chu, H.; Yang, Y.; Zhang, Q.; Wang, Y. *J. Catal.* **2006**, *241*, 225–228.

- (20) Suo, Z. H.; Jin, M. S.; Lu, J. Q.; Wei, Z. B.; Li, C. *J. Nat. Gas Chem.* **2008**, *17*, 184–190.
- (21) Bauer, J. C.; Veith, G. M.; Allard, L. F.; Oyola, Y.; Overbury, S. H.; Dai, S. *ACS Catal.* **2012**, *2*, 2537–2546.
- (22) Liu, P.; Hensen, E. J. M. *J. Am. Chem. Soc.* **2013**, *135*, 14032–14035.
- (23) Perdew, J. P.; Burke, K.; Ernzerhof, M. *Phys. Rev. Lett.* **1996**, *77*, 3865–3868.
- (24) Kresse, G.; Furthmuller, J. *Comput. Mater. Sci.* **1996**, *6*, 15–50.
- (25) Kresse, G.; Furthmuller, J. *Phys. Rev. B* **1996**, *54*, 11169–11186.
- (26) Kresse, G.; Hafner, J. *Phys. Rev. B* **1993**, *47*, 558–561.
- (27) Dudarev, S. L.; Botton, G. A.; Savrasov, S. Y.; Humphreys, C. J.; Sutton, A. P. *Phys. Rev. B* **1998**, *57*, 1505–1509.
- (28) Blöchl, P. E. *Phys. Rev. B* **1994**, *50*, 17953–17979.
- (29) Kresse, G.; Joubert, D. *Phys. Rev. B* **1999**, *59*, 1758–1775.
- (30) Bengone, O.; Alouani, M.; Blöchl, P. E.; Hugel, J. *Phys. Rev. B* **2000**, *62*, 16392–16401.
- (31) Xiang, H. J.; Kan, E. J.; Wei, S.; Whangbo, M. H.; Gong, X. Q. *Phys. Rev. B* **2011**, *84*, 224429.
- (32) Song, W. Y.; Liu, P.; Hensen, E. J. M. *Catal. Sci. Technol.* **2014**, *4*, 2997–3003.
- (33) (a) Molina, L. M.; Rasmussen, M. D.; Hammer, B. *J. Chem. Phys.* **2004**, *120*, 7673–7680. (b) Green, I. X.; Tang, W.; Neurock, M.; Yates, J. T. *Science* **2011**, *333*, 736–739.
- (34) Henkelman, G.; Uberuaga, B. P.; Jonsson, H. *J. Chem. Phys.* **2000**, *113*, 9901–9904.
- (35) Kemei, M. C.; Barton, P. T.; Moffit, S. L.; Gaulois, M. W.; Joshua, A.; Seshadri, R.; Matthew, R.; Kim, Y. I. *J. Phys.: Cond. Matter* **2013**, *25*, 326001.
- (36) Nijhuis, T. A.; Sacaliuc, E.; Beale, A. M.; van der Eerden, A. M.; Schouten, J. C.; Weckhuysen, B. M. *J. Catal.* **2008**, *258*, 256–264.
- (37) Pease, R. N. *J. Am. Chem. Soc.* **1923**, *45*, 1196–1210.
- (38) Kistiakowsky, G. B.; Ruhoff, J. R.; Smith, H. A.; Vaughan, W. E. *J. Am. Chem. Soc.* **1935**, *57*, 876–882.
- (39) Sussman, M. V.; Potter, C. *Ind. Eng. Chem.* **1954**, *46*, 457–465.
- (40) Hayashi, T.; Tanaka, K.; Haruta, M. *J. Catal.* **1998**, *178*, 566–575.
- (41) Duma, V.; Hönigke, D. *J. Catal.* **2000**, *191*, 93–104.
- (42) Gu, J.; Yan, Y.; Krizan, J. W.; Gibson, Q. D.; Detweiler, Z. M. D.; Cava, R. J.; Bocarsly, A. B. *J. Am. Chem. Soc.* **2014**, *136*, 830–833.
- (43) (a) Ozbek, M. O.; van Santen, R. A. *Catal. Lett.* **2013**, *143*, 131–141. (b) Linic, S.; Barteau, M. A. *J. Am. Chem. Soc.* **2003**, *125*, 4034–4035. (c) Bocquet, M. L.; Loffreda, D. *J. Am. Chem. Soc.* **2005**, *127*, 17207–17215.
- (44) Lei, Y.; Mehmood, F.; Lee, S.; Greeley, J.; Lee, B.; Seifert, S.; Winans, R. E.; Elam, J. W.; Meyer, R. J.; Redfern, P. C.; Teschner, D.; Schlögl, R.; Pellin, M. J.; Curtiss, L. A.; Vajda, S. *Science* **2010**, *328*, 224–228.